A NEW UNCOUPLED VISCOPLASTIC CONSTITUTIVE MODEL*

Walter L. Bradley and Shik Yuen
Texas A&M University
College Station, Texas 77843

INTRODUCTION

A new uncoupled viscoplastic model has been developed which assumes a portion of the inelastic strain is rate independent (or at least rate insensitive). Unlike earlier uncoupled models, this model recognizes that some of the inelastic strain which occurs during a load change is rate sensitive (or thermally activated). To separate the rate dependent and rate independent contributions, hysteresis loops are run in strain control at temperatures that are sufficiently low that essentially identical loops are obtained for a 40s, 120s, and 1200s period. This $\sigma - \varepsilon$ loop is assumed to define the stress/rate-insensitive, inelastic strain behavior for all temperatures. Subsequent tests at higher temperatures will include rate-sensitive and rate-insensitive components of inelastic strain. However, since the magnitude of the rate-insensitive inelastic strain at each stress and temperature is already known from the low temperature hystersis loop measurements, the rate sensitive inelastic strain component can be determined by subtraction. The stress/rate-sensitive, inelastic strain is then modelled using standard viscoplastic models.

At higher temperatures, and therefore, lower stresses, the rate independent inelastic strain contribution is found to be negligible and the predictions of the model are exactly those of standard viscoplastic models. However, at lower temperatures and the resultant higher stresses, the rate independent, inelastic strain is significant and accounts for the rounded corners that are currently a problem for viscoplastic models which assume all inelastic strain to be rate sensitive.

In this paper we will present the physical basis for the uncoupled viscoplastic model, describe the various experiments used to evaluate the material constants, and compare predictions of stress relaxation behavior by the model to experimental results where the material constants have been determined using hysteresis loop data.

PHYSICAL BASIS FOR MODEL

Deformation of metals and alloys occurs by dislocation glide, cross-slip and climb. Additional flow may result from grain boundary sliding, though some dislocation deformation in the grains

* This work was sponsored by NASA under direction of Dr. Robert Thompson

is required even here for compatibility. In the low temperature regime (0-0.20T_m), the yield strength and flow stress are found to vary significantly with temperature. This is particularly true for materials with a body centered cubic lattice structure. The fairly small activation energy for thermally assisted dislocation motion at these low temperatures is usually associated with dislocations overcoming lattice friction (Peirels stress) or possibly dislocation intersections.

Between 0.20-0.40T_m, the thermal assistance to overcoming such barriers is more than adequate, allowing dislocation glide to occur equally easily at various temperatures and/or strain rates in this temperature range. Here, the flow stress depends more on the inelastic strain and the resultant strain hardening it produces than on the strain-rate. While short range barriers to glide such as Peirels stress are easily overcome with thermal assistance at these temperatures, the thermal energy is relatively small and generally ineffective in giving much thermally assisted recovery via dislocation cross-slip, climb, etc. The activation barriers for such processes are relatively large compared to the phonon energies (thermal energy), making these processes quite sluggish; thus, their contribution to the overall deformation is quite small. In summary, between 0.20 and 0.4T_m, thermally activated processes are either so rapid (e.g., overcoming Peirels stress) or so slow(e.g., dislocation climb) that very little rate sensitivity observed over this temperature range. We may say the deformation behavior in this temperature range is rate insensitive and over a range of strain-rates of 50-100X will be essentially rate independent. It will be shown later that Hastelloy-X specimens tested under fully reversible strain conditions over a temperature range of 298K to 533K (0.2 to 0.35T_m) and over a 30X strain-rate range (9.70×10^{-4} to 3.23×10^{-5} s^{-1})[n] at each temperature have essentially identical hysteresis loops and material constants for Ω and K. At 755K (0.49T_m), the hysteresis loop is changing slightly, though rate dependence over the strain-rate range (30X) we have studied is still not significant.

As the specimen deformation temperature is raised above 0.5T_m, rate sensitive, inelastic deformation becomes apparent. Hysteresis loop size (and shape to a degree) changes with changing strain-rate. At these higher temperatures, thermally activated cross-slip and climb now becomes possible, particularly at the slower strain-rates, which lowers the peak stress achievable in the hysteresis loop. We will associate our rate sensitive, inelastic strain with the additional increments of deformation made possible by the thermally assisted overcoming of these larger barriers to deformation, i.e., dynamic recovery, or softening. The rate sensitivity is seen principally in the circumventing of various barriers by cross-slip or climb rather than in the subsequent glide to the next barrier. Nevertheless, all of the inelastic strain that results from the combined cross-slip (or climb) and subsequent glide will be included in the rate sensitive, inelastic strain.

We have implicitly divided our inelastic strain into a component which results in strain hardening and a component which does not. Even during the portion of the hysteresis loop where strain hardening is occuring, the inelastic strain may contain rate dependent (no strain hardening) as well as rate independent (strain hardening) components. It should be emphasized that net strain hardening continues until the back stress reaches a level where recovery and strain hardening are balanced. Ideally, the stress is dependent on the rate insensitive, inelastic strain and the rate sensitive, inelastic strain-rate. A transient dependence of stress on the rate sensitive, inelastic strain (as well as strain-rate) is sometimes observed and is equivalent to primary creep. Since we are initially interested in modelling hysteresis loop behavior for saturated loops, such transients are not expected to be significant. They do probably play a role in the initial "shakedown" where dislocations are gradually being rearranged into more stable cell structure configurations.

In summary, we believe that the inelastic strain may be uncoupled into two components, one associated principally with dislocation glide resulting in strain hardening and a second associated with dynamic recovery processes including dislocation cross-slip and climb. To a first approximation, the flow stress should depend on the rate insensitive, inelastic strain and the rate dependent, inelastic strain-rate. The stress/rate- sensitive inelastic strain-rate relationship can be modelled using viscoplastic models. The stress/rate-insensitive, inelastic strain relationship is determined from hysteresis loops taken at a suitably low temperature ($0.2-0.3T_m$). At higher temperatures, the flow stress is relatively low and the inelastic strain is essentially all rate-sensitive, resulting from dynamic recovery processes. At lower temperatures and the resultant higher flow stresses, a significant portion of the total inelastic strain will be rate insensitive deformation. The more gently rounded corners of the hysteresis loop observed at these temperatures are a consequence of this rate-insensitive, inelastic strain.

In this next section, the constitutive model will be defined in mathematical equations and the experiments required to characterize the various constants will be described.

CONSTITUTIVE MODEL

The total strain-rate is assumed to be divisible into three components; an elastic component $\dot{\varepsilon}_e$, a rate-insensitive inelastic component $\dot{\varepsilon}_{ii}$, and a rate-sensitive inelastic component $\dot{\varepsilon}_{ir}$; i.e.

$$\dot{\varepsilon}_t = \dot{\varepsilon}_e + \dot{\varepsilon}_{ii} + \dot{\varepsilon}_{ir} \qquad (1)$$

The rate-sensitive strain rate $\dot{\varepsilon}_{ir}$ is modelled using the relationship typically used in unified theories for inelastic strain rate (note unified theory assumes all inelastic strain is rate sensitive); namely,

$$\dot{\varepsilon}_{ir} = \left(\frac{\sigma-\Omega}{K}\right)^n \qquad (2)$$

where σ is the applied stress, Ω is the back stress and K is the drag stress. The elastic strain-rate is modelled in the usual way as

$$\dot{\varepsilon}_e = \dot{\sigma}/E \tag{3}$$

Finally, the rate-insensitive, inelastic strain is modelled with an empircally determined strain hardening function $f(\sigma,\sigma_{max})$ as follows:

$$\dot{\varepsilon}_{ii} = f(\sigma, \sigma_{max})\,\dot{\sigma} \tag{4}$$

where $f(\sigma,\sigma_{max}) = \frac{d\varepsilon_{ii}}{d\sigma}$ as measured from hysteresis loops for different strain ranges, and therefore, σ_{max} values, as shown in Figure 1. It should be noted that the hystersis loops even at these lower temperatures are slightly asymmetric so the sign of the σ_{max} before the stress reversal as well as its magnitude must be specified to define the particular f value for a given value of σ in a stress reversal. The results for $f(\sigma,\sigma_{max})$ determined from the data in Figure 1 is summarized in Table 1. The stress-rate may be calculated from Equations (1)-(4) for a given axial strain-rate of $\dot{\varepsilon}_t$ as follows:

$$\dot{\sigma} = \frac{\dot{\varepsilon}_t - \left(\frac{\sigma-\Omega}{K}\right)^n}{\frac{1}{E} + f(\sigma, \sigma_{max})} \tag{5}$$

or

$$\Delta\sigma = \frac{\Delta\varepsilon_t - \left(\frac{\sigma-\Omega}{K}\right)^n \Delta t}{\frac{1}{E} + f(\sigma, \sigma_{max})} \tag{6}$$

The evaluation of $\Delta\varepsilon_t$ is given by $\dot{\varepsilon}_t \Delta t$ where the total axial strain-rate for a constant diametral strain rate dD/dt is

$$\dot{\varepsilon}_t = \frac{\frac{-2}{D_0}\frac{dD}{dt}}{1 - \frac{1}{E}\frac{d\sigma}{d\varepsilon}(1-2\nu)} \tag{7}$$

It should be noted that the appropriate time step Δt is selected by monotonically decreasing the value of Δt until the simulated σ-ε hysteris loops for two successive choices of Δt are essentially identical.

The material constants which must be determined empirically in Equation 5 are $\Omega(\sigma,T,N)$, $K(\sigma,T,N)$, $E(T)$, $f(\sigma,\sigma max)$ and $n(T)$ where N and T refer to the cycle number and temperature respectively. For the initial phase of this program, we chose to evaluate only saturated hystersis loop behavior, eliminating for the moment "N" as a variable. It was further assumed that for a saturated hystersis loop, "K" would retain a constant value around the loop whereas Ω was assumed to vary with σ around the loop. The rational for this assumption is that the drag stress is physically associated with the dislocation cell structure, or dislocations in stable configurations while Ω is associated with the metastable dislocation arrangements such as pileups, multiple loops around particles, etc. Once a stable dislocation cell structure is formed (i.e., at saturation), it is reasonable to assume it does not change appreciably as we traverse a strain cycle. It may also be reasonably expected that the cycle to cycle changes leading to saturation will be associated with an N dependence of K, with Ω independent of N, at least to a first approximation.

Stress relaxation tests were made in an attempt to determine "n" and "Ω" over the entire range of temperatures studied (755K-1144K). Using an analysis first suggested by J.C.M. Li (1), it was determined that the back stress decreased significantly during the stress relaxation tests for temperatures of 978K (1300°F) and above, giving erroneous results for both "n" and "Ω". This was subsequently confirmed by drop stress/strain transient tests used to measure the back stress. Thus, stress relaxation tests were only used over the temperature range of 755K-922K to determine "n" and "Ω". At higher temperatures (978K-1144K), stress drop/strain transient tests were used to determine the back stress Ω. Then abrupt strain-rate change tests were used to determine the value of "n". The strain-rate was decreased by a factor of 3x and by a factor of 30x with the resultant flow stress measured. It was assumed that "K" remained constant during these strain-rate changes but that "Ω" changed to a new value during 0.5s transient that occured before a new "steady-state" flow stress was attained. The plotting of (σ-Ω) vs. $\dot{\varepsilon}_{ir}$ allowed the stress exponent "n" to be evaluated.

At all temperatures, "K" was subsequently evaluated using Equation 2 at the same stress where "n" and "Ω" had previously been evaluated (usually on the plateau of the hysteresis loop or near σ_{max} at lower temperatures where no plateau was reached). With n, Ω, and K determined for one σ-ε position on the hysteresis loop and assuming n and K are constant for a saturated loop at a given temperature and strain-rate, one may then calculate Ω for other points around the hysteresis loop using Equation 2. Typical results for Ω vs. ε(orσ) are shown in Figure 2.

EXPERIMENTAL PROCEDURES AND DATA REDUCTION

Round tensile bars with a gage section 4 cm long by 1 cm in diameter were prepared from Hastelloy-X. They were then inserted into a 100 Kip MTS materials testing system with special water cooled grips and a diametral extensometer which utilizes quartz rods. Induction heating was used with an Ircon optical controller to heat the specimens. The temperature variaton at 1144K was ±1.1K. An absolute accuracy of ±3K was attained by calibrating the optical controller using Hastelloy-X in a conventional furnace. High purity thermocouple wires and a precision digital thermometer were used to establish the actual temperature. Several thermocouples were used to verify the absence of significant temperature gradients in the small Hastelloy-X specimen used in calibration as well as in the tensile specimens' gage length during temperature maintenance by induction heating. The calibration of the optical controller is checked every three months and recalibrated as needed.

Special alignment procedures were used to reduce an initial variation in axial strain measurements at three equally spaced positions around the circumference from 30% to 5% maximum. This was verified on several successive specimens and then was not checked thereafter. Only one specimen was buckled in testing, and this specimen had a fatigue crack which had grown across about 20% of the cross-section.

Specimens were tested at ten temperatures ranging from 298K ($0.20T_m$) to 1144K ($0.75T_m$). At each temperature, specimens were tested at three diametral strain-rates with gage axial strain-rates of approximately 10, 3.3 and $0.33 \times 10^{-4} s^{-1}$, the instantaneous strain-rate varying slightly around these values depending on the relative amounts of elastic and inelastic strain. The strain range used was ±1% axial strain and the specimens were cycled until the loop saturated, which required as few as two cycles at higher temperatures but as many as 40-50 cycles at lower temperatures.

Diameter measurements were converted into total axial strain using the easily derived relationship

$$\varepsilon_t = \frac{\sigma}{E}(1 - 2\nu) - 2\frac{\Delta D}{D_o} \qquad (8)$$

where E and ν are the elastic modulus and Poisson's ratio, D_o is the initial diameter and ΔD is the change in diameter. The axial inelastic strain is easily calculated as the difference in the total strain and the elastic strain,

or

$$\varepsilon_i = \frac{-2\nu\sigma}{E} - \frac{2\Delta D}{D_o} \qquad (9)$$

Equations for the total strain rate $\dot{\varepsilon}_t$ and the inelastic strain rate $\dot{\varepsilon}_i$ are also easily derived in terms of the measured load/diameter relationships and give

$$\dot{\varepsilon}_t = \frac{\frac{-2}{D_o}\frac{dD}{dt}}{1 - \frac{1}{E}\frac{d\sigma}{d\varepsilon_t}(1-2\nu)} \qquad (10)$$

$$\dot{\varepsilon}_i = \frac{-2}{D_o}\frac{dD}{dt}\left[\frac{1 - \frac{1}{E}\frac{d\sigma}{d\varepsilon_t}}{1 - \frac{(1-2\nu)}{E}\frac{d\sigma}{d\varepsilon_t}}\right] \qquad (11)$$

where

$$\frac{d\sigma}{d\varepsilon_t} = \frac{1}{\left(\frac{1-2\nu}{E} - \frac{2}{D_o}\frac{dD}{d\sigma}\right)} \tag{12}$$

Since $\frac{dD}{dt}$ is specified in programming the MTS function generator and $dD/d\sigma$ is easily measured, the total and inelastic strain-rates $\dot{\varepsilon}_t$ and $\dot{\varepsilon}_i$ are also easily determined from load/diameter measurements.

With the strain hardening function $f(\sigma,\sigma_{max})$ defined from hysteresis loops at lower temperatures where all inelastic strain is rate insensitive, Equation 4 can be used to quantify the rate insensitive inelastic strain-rate for any temperature and stress rate, $\dot{\sigma}$. Since the total inelastic strain-rate may be calculated from Equation (11) and the rate insensitive strain-rate calculated through using Equation (4), the rate sensitive strain-rate is easily calculated as the differnce in these two quantities. Thus, the elastic, inelastic rate-insensitive and inelastic rate-sensitive contributions to the total strain-rate may all be evaluated from the experimentally measured load-displacement curves. Once the rate-sensitive component of strain-rate is evaluated, the Ω can be calculated for various measured values of σ and calculated values of "n" and "K".

The stress relaxation tests were run under constant diameter conditions imposed by interrupting the diametral strain cycling at various points on the hysteresis loop. The stress-time response during the interruption of strain cycling is measured using a second recorder so as to not interfere with the load-diameter measurements. The axial, rate-sensitive strain-rate is determined from the load time record using the relationship

$$\dot{\varepsilon}_{ir} = \frac{-2\nu}{E}\dot{\sigma} \tag{13}$$

derived assuming stress relaxation under constant diameter conditions. Load versus dP/dt is taken and used to evaluate $\dot{\varepsilon}_{ir}$. The value for "n" in Equation 2 may be determined by plotting $\ln \dot{\varepsilon}_{ir}$ vs. $\ln(\sigma-\Omega)$. assuming Ω does not change during the test.

Experimental Results and Discussion

Typical stress/total strain and stress/ rate-sensitive inelastic strain results are seen in Figures 3 and 4 respectively. Results at room temperature ($0.20T_m$) and 533K($0.35T_m$) at three strain-rates gave essentially identical hysteresis loops, indicating the inelastic strain over this temperature range is all rate insensitive. Additional hystersis loops were run at room temperature for strain amplitudes of ± 0.05%, 0.1%, 0.2%, 0.3%, 0.4%, 0.6%, 0.8%, with the ± 1% having been run previously. These results are presented in Figure 1 with the $f(\sigma,\sigma_{max})$ values tabulated in Table 1.

The various material constants required for characterization of the rate sensitive, inelastic strain are summarized in Table II. The elastic constants as a function of temperature are summarized in Table III. It should be noted in Table II that "n" varies from 3.63 to 5.57. This is in sharp contrast to unified models where the "n" value at lower temperatures may be as high as 60-100. We too found "n" values of 50-100 if we ran strain-rate cycling tests at lower temperatures and analyzed the results assuming all of the inelastic strain was rate sensitive (or rate dependent) as the unified theory does.

The back stress is seen to increase with increasing stress as one might expect. At higher temperatures, the slower strain-rate gives the lower back stress. At temperatures below 978K, the back stress does not seem to be a sensitive function of strain-rate. At 978K and above "K" is seen to systematically decrease with increasing temperature. This indicates an increasing mobile dislocation density, possibly resulting from an increased cell size which is both the source of mobile dislocations and a place where they may be entrapped. At lower temperatures "K" increases with decreasing strain-rate, again indicating the expected lower mobile dislocation density at lower strain-rates. These differences in calculated "K" are a result of stress relaxation data for different prior strain-rates being displaced vertically in a $\ln \dot{\varepsilon}_{ir}$ vs. $\ln(\sigma-\Omega)$ plot. The constant "K" values at various strain-rates at higher temperatures are assumed in the analysis, this assumption being justified by a careful analysis of the strain-rate cycling tests.

Table IV summarizes the results of analysis of the inelastic strain-rate just before and just after the strain cycling is interrupted for a stress relaxation test. The inelastic strain is given from equations (1), (2) and (4) as

$$\dot{\varepsilon}_{ii} + \dot{\varepsilon}_{ir} = f(\sigma, \sigma_{max})\,\dot{\sigma} + \left(\frac{\sigma-\Omega}{K}\right)^n \qquad (14)$$

Since $\dot{\sigma}$ goes from positive to negative as one interrupts the strain cycling for stress relaxation and since $f(\sigma, \sigma_{max})$ is essentially zero just after a load reversal, the rate insensitive strain-rate experiences a discontinuous change from a positive value to zero. Since the stress is continuous at this time, one would expect the rate-sensitive inelastic strain-rate to be continuous. Thus, a large decrease in inelastic strain-rate as one interrupts the strain cycling indicates that the inelastic strain-rate during strain cycling is principally rate-insensitive. If the inelastic strain-rate before and after the interruption is essentially the same, this indicates that the inelastic strain during cyclic straining must have been essentially all rate sensitive. Thus, inelastic strain-rate continuity is a good measure of to what degree the inelastic strain is rate sensitive. A large discontinuity indicates significant rate-insensitive strain. Table IV summarizes such results over a wide range of strain rates and temperatures. The trends as expected show a greater degree of rate-dependent inelastic-strain (smaller discontinuity) for higher temperatures and slower strain-rates. These results show a gradual transition from about 100% rate insensitive flow at high strain-rates and lower temperatures (as in classical plasticity) to 100% rate sensitive flow as in the unified theories. It should be noted that our constitutive model will cover this entire range as it explicitly accounts for both types of inelastic strain.

PREDICTIONS

The constitutive model as described in Equations 1-4 and reformulated into Equations 5-7 may be used to predict strain cycling, stress relaxation or other phenomena if used with the approximate material constants. Such constants for Hastelloy-X are summarized in Tables I, II and III. To first see if the model is self consistent in being able to predict the original strain cycling curves from which Tables I, II and III were determined, all of the input strain cycling curves were simulated using Equations 6 and 7 and the material constants in Tables I, II and III. The original curves and the simulated curves were found to be in excellent agreement over the whole range of temperatures and strain-rates, as seen in the selected examples presented in Figure 5. Gently rounded corners are well simulated at the lower temperatures using this uncoupled approach. The unified theory with its high "n" values always gives square corners at lower temperatures.

Stress relaxation simulations are presented in Figure 6. At the lower temperature, the results are reasonable; however, at the higher temperature the actual asymptotic stress value is much lower than the predicted one. This is because we have not yet accounted for thermal recovery of our state variables Ω and K. The back stress does decrease during stress relaxation at higher temperatures as has been previously noted. We are still assuming a constant value for Ω and K during stress relaxation.

SUMMARY

A new uncoupled viscoplastic model has been proposed along with experiments and analysis to define the various material constants. Distinguishing between rate sensitive and rate insensitive strain allows the rate sensitive strain to be modelled over a wide range of temperatures with very little variation in the stress component "n". Furthermore, it allows the rounded corners on stress-strain hysteresis loops to be achieved very naturally.

Table I. Values for Rate Independent, Inelastic Strain Function $f(\sigma,\sigma_{max})$

σ(MPa)	$f(\sigma,\sigma_{max})\,MPa^{-1}$
for σ_{max} = 149 MPa	
Loading	
-149	0
-106	0
106	0
149	0
Unloading	
149	0
106	0
-106	0
-149	0
for σ_{max} = 286	
Loading	
-286	0
0	0
106	0.187E-6
212	0.406E-6
286	0.161E-5
Unloading	
286	0
0	0
-106	0.275E-6
-212	0.580E-6
-286	0.148E-5
for σ_{max} = 392 MPa	
Loading	
-403	0
0	0.319E-6
106	0.165E-5
212	0.259E-5
318	0.435E-5
392	0.124E-4
Unloading	
392	0
0	0.232E-6
-106	0.186E-5
-212	0.270E-5
-318	0.417E-5
-403	0.107E-4
for σ_{max} = 435 MPa	
Loading	
-446	0
0	0.652E-6
106	0.258E-5
212	0.432E-5
318	0.620E-5
392	0.126E-4
424	0.246E-4
435	0.680E-4
Unloading	
435	0
0	0.551E-6
-106	0.214E-5
-212	0.441E-5
-318	0.694E-5
-392	0.108E-4
-424	0.184E-4
-446	0.522E-4

σ(MPa)	$f(\sigma,\sigma_{max})\,MPa^{-1}$
for σ_{max} = 467 MPa	
Loading	
-477	0
-106	0.145E-6
0	0.113E-5
106	0.255E-5
212	0.559E-5
318	0.880E-5
424	0.187E-4
461	0.455E-4
467	0.134E-3
Unloading	
467	0
106	0.145E-7
0	0.104E-5
-106	0.294E-5
-212	0.546E-5
-318	0.890E-5
-424	0.165E-4
-459	0.329E-4
-477	0.913E-4
for σ_{max} = 520 MPa	
Loading	
-530	0
-106	0.681E-6
0	0.164E-5
106	0.330E-5
212	0.732E-5
318	0.114E-4
424	0.197E-4
477	0.333E-4
509	0.754E-4
520	0.196E-3
Unloading	
520	0
106	0.127E-6
0	0.135E-5
-106	0.383E-5
-212	0.723E-5
-318	0.110E-4
-424	0.177E-4
-477	0.310E-4
-509	0.541E-4
-530	0.157E-3
for σ_{max} = 562 MPa	
Loading	
-567	0
-106	0.986E-6
0	0.225E-5
106	0.394E-5
212	0.658E-5
265	0.862E-5
318	0.126E-4
371	0.164E-4
424	0.220E-4
477	0.328E-4
509	0.461E-4
530	0.600E-4
552	0.111E-3
562	0.291E-3

σ(MPa)	$f(\sigma,\sigma_{max})\,MPa^{-1}$
for σ_{max} = 562 MPa	
Unloading	
562	0
106	0.783E-6
0	0.174E-5
-106	0.388E-5
-212	0.677E-5
-318	0.120E-4
-371	0.164E-4
-424	0.217E-4
-477	0.314E-4
-509	0.403E-4
-530	0.565E-4
-546	0.796E-4
-557	0.132E-3
-567	0.388E-3
for σ_{max} = 610 MPa	
Loading	
-615	0
-106	0.141E-5
0	0.288E-5
106	0.429E-5
212	0.723E-5
318	0.126E-4
371	0.175E-4
424	0.232E-4
477	0.307E-4
530	0.448E-4
562	0.629E-4
583	0.868E-4
605	0.162E-3
610	0.229E-3
Unloading	
610	0
106	0.681E-6
0	0.188E-5
-106	0.367E-5
-212	0.630E-5
-318	0.103E-4
-371	0.159E-4
-424	0.194E-4
-477	0.274E-4
-530	0.416E-4
-562	0.572E-4
-583	0.894E-4
-605	0.186E-3
-615	0.372E-3

Table II. Values for Back Stress(for $\sigma = \sigma_{max}$), n, Drag Stress(K) and K^n

Temp. (K)	Temp. (°F)	Ω (MPa) strain rate ($10^{-4}s^{-1}$) 10	3.3	0.33	n	K ($MPa\,s^{1/n}$) strain rate ($10^{-4}s^{-1}$) 10	3.3	0.33	K^n ($MPa^n S$) strain rate ($10^{-4}s^{-1}$) 10	3.3	0.33
755	900	468	468	474	5.50	390	513	1045	1.78×10^{14}	8.05×10^{14}	4.03×10^{16}
810	1000	252	265	318	4.96	1186	1260	1704	1.77×10^{15}	2.39×10^{15}	1.07×10^{16}
866	1100	255	226	237	5.57	905	978	1274	2.94×10^{16}	4.53×10^{16}	1.98×10^{17}
922	1200	161	164	163	4.31	1690	1829	2597	8.17×10^{13}	1.15×10^{14}	5.20×10^{14}
978	1300	141	136	115	5.57	800	800	800	1.48×10^{16}	1.48×10^{16}	1.48×10^{16}
1033	1400	118	111	82	4.75	672	672	672	2.69×10^{13}	2.69×10^{13}	2.69×10^{13}
1089	1500	76	66	43	4.70	488	488	488	4.32×10^{12}	4.32×10^{12}	4.32×10^{12}
1144	1600	41	38	28	3.63	532	532	532	7.85×10^{9}	7.85×10^{9}	7.85×10^{9}

900°F - 1200°F: Ω, n & K obtained from stress relaxation tests.

1300°F - 1600°F: n obtained from strain rate change test
Ω obtained from stress drop tests.
K assumed to be constant for all strain rates

Table III. Values for Young's Modulus and Poisson's Ratio

Temp. (K)	Temp. (°F)	Temp. (C°)	T/T_m*	(10^6psi)	E(GPa)
294	70	21	0.19	28.6	197
533	500	260	0.35	26.3	182
755	900	482	0.49	24.0	166
810	1000	538	0.53	23.4	162
866	1100	593	0.57	22.8	158
922	1200	649	0.60	22.3	154
978	1300	704	0.64	21.7	150
1033	1400	760	0.67	21.1	146
1089	1500	816	0.71	20.5	142
1144	1600	871	0.75	19.9	137

ν = 0.32 (assumed constant for all temp.)

*melting range is 1260-1255°C

Table IV. Inelastic Strain Rate Continuity at Various Temperatures

$\dot{\varepsilon}_t = 1 \times 10^{-3} s^{-1}$ (10S/½ cycle)

$\dot{\varepsilon}_t = 3.3 \times 10^{-4} s^{-1}$ (30S/½ cycle)

$\dot{\varepsilon}_t = 3.3 \times 10^{-5} s^{-1}$ (300S/½ cycle)

A) $\dot{\varepsilon}_t = 1 \times 10^{-3} s^{-1}$

Temp. (K)	Temp. (°F)	σ (MPa)	$\dot{\varepsilon}p^-$ $(10^{-4}s^{-1})$	$\dot{\varepsilon}p^+$ $(10^{-4}s^{-1})$	$\dot{\varepsilon}p^+/\dot{\varepsilon}p^-$ (%)
755	900	434 558	8.76 9.57	.21 .10	2 1
810	1000	492	9.51	1.22	13
866	1100	386 455	9.18 9.57	2.12 1.01	23 11
922	1200	405 458	9.34 9.59	2.34 1.95	25 20
978	1300	330	9.40	9.01	96
1033	1400	277	9.80	9.80	100
1089	1500	185	9.61	9.61	100
1144	1600	119	9.83	9.83	100

$\dot{\varepsilon}p^-$ = plastic strain rate before the beginning of stress relaxation test

$\dot{\varepsilon}p^+$ = plastic strain rate after the beginning of stress relaxation test

B) $\dot{\varepsilon}_t = 3.3 \times 10^{-4} s^{-1}$

Temp. (K)	Temp. (°F)	σ (MPa)	$\dot{\varepsilon}p^-$ $(10^{-4}s^{-1})$	$\dot{\varepsilon}p^+$ $(10^{-4}s^{-1})$	$\dot{\varepsilon}p^+/\dot{\varepsilon}p^-$ (%)
755	900	450 568	2.95 3.19	.41 .24	14 8
810	1000	394 471	2.98 3.16	.40 .69	13 22
866	1100	376 439	3.10 3.20	.68 .54	22 17
922	1200	381 431	3.14 3.22	1.21 1.38	39 43
978	1300	327	3.19	3.09	97
1033	1400	236	3.27	3.27	100
1089	1500	154	3.21	3.21	100
1144	1600	96	3.29	3.29	100

c) $\dot{\varepsilon}_t = 3.3\text{x}10^{-5}s^{-1}$

Temp. (K)	Temp. (°F)	σ (MPa)	$\dot{\varepsilon}p^-$ ($10^{-5}s^{-1}$)	$\dot{\varepsilon}p^+$ ($10^{-5}s^{-1}$)	$\dot{\varepsilon}p^+/\dot{\varepsilon}p^-$ (%)
755	900	592	3.19	.82	26
810	1000	373	2.97	.80	27
866	1100	354	3.05	1.84	60
922	1200	352	3.15	2.38	76
978	1300	246	3.20	3.19	100
1033	1400	163	3.27	3.27	100
1089	1500	100	3.22	3.22	100
1144	1600	59	3.29	3.29	100

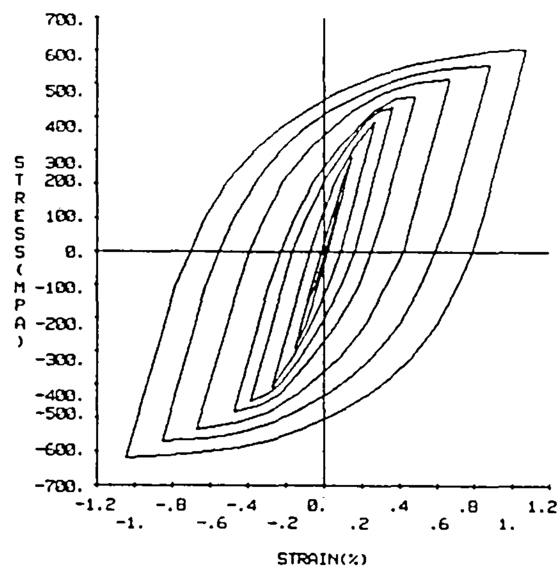

Figure 1. Saturated stress-strain results for Hastelloy-X at room temperature for total strain amplitudes of 0.05%,0.1%,0.2%, 0.3%,0.4%,0.5%,0.6%,0.8%,1.0%.

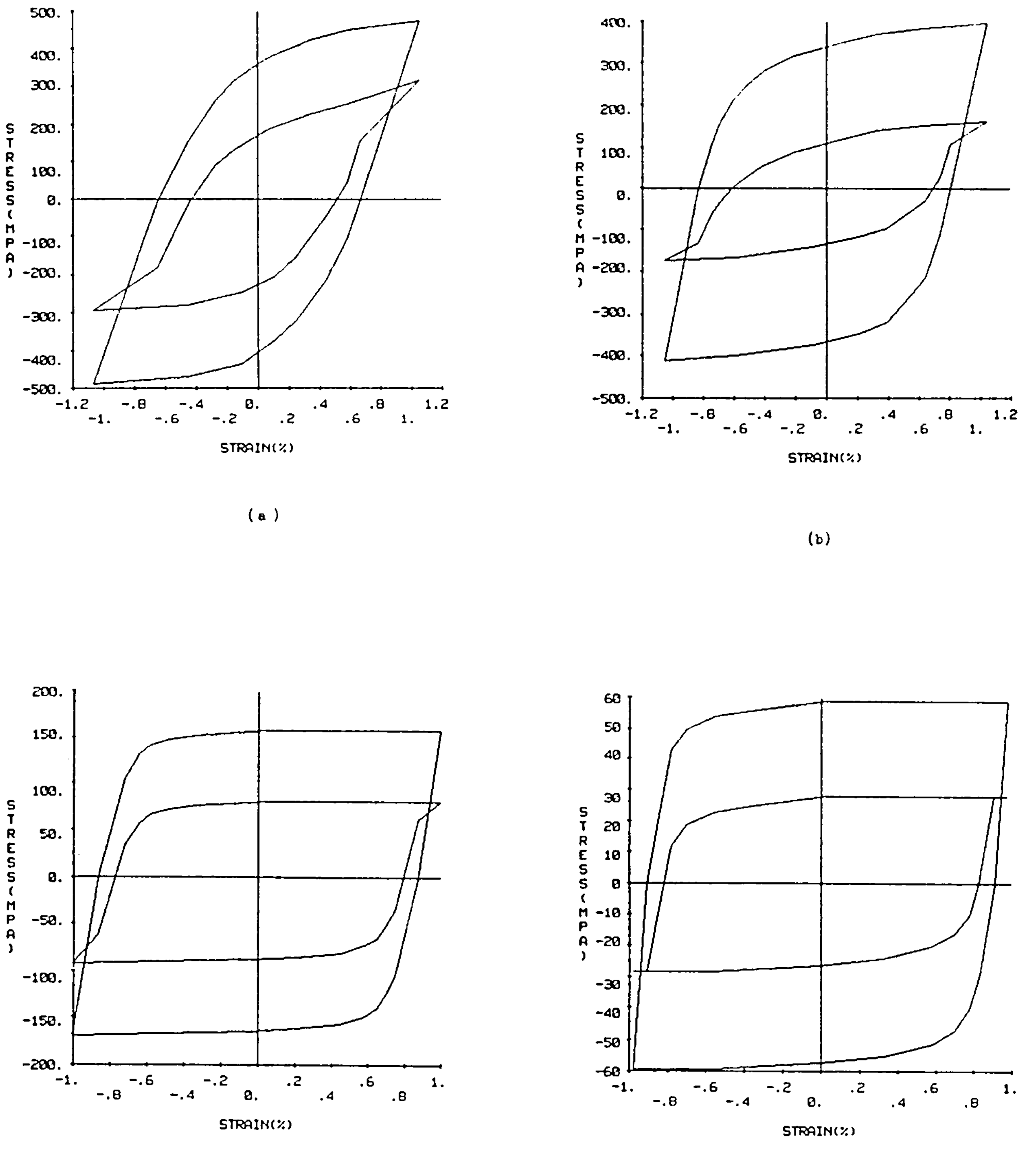

Figure 2. Stress and back stress as a function of strain as calculated from model for a) 810K and $\dot{\varepsilon}=3.3\mathrm{X}10^{-5}s^{-1}$; b) 922K and $\dot{\varepsilon}=3.3\mathrm{X}10^{-5}s^{-1}$; c) 1033K and $\dot{\varepsilon}=3.3\mathrm{X}10^{-5}s^{-1}$; d) 1144K and $\dot{\varepsilon}=3.3\mathrm{X}10^{-5}s^{-1}$.

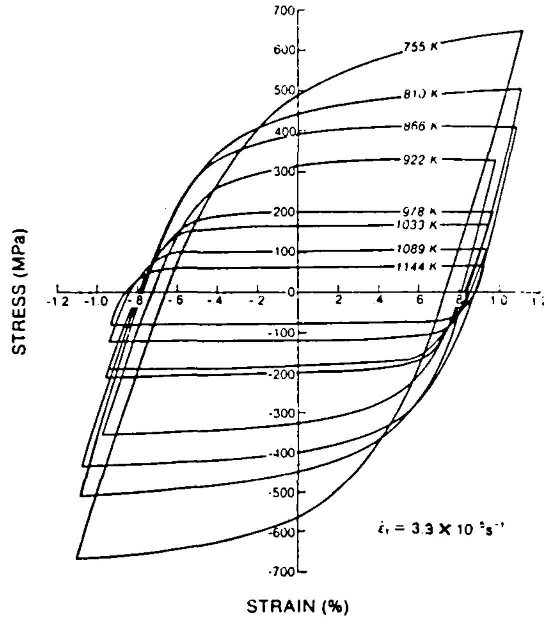

Figure 3. Saturated hysteresis loops of stress vs. total strain for Hastelloy-X at various temperatures.

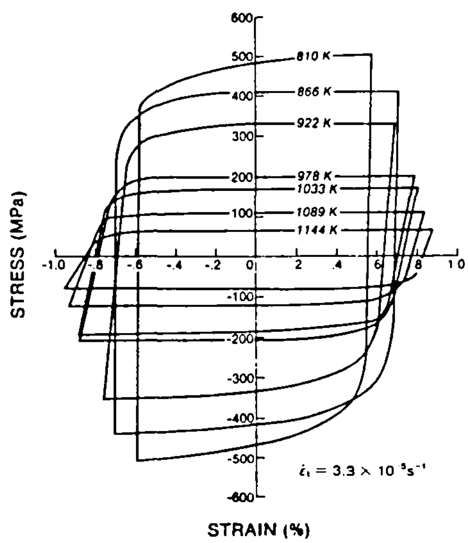

Figure 4. Saturated hysteresis loops of stress vs. rate dependent inelastic strain for Hastelloy-X at various temperatures.

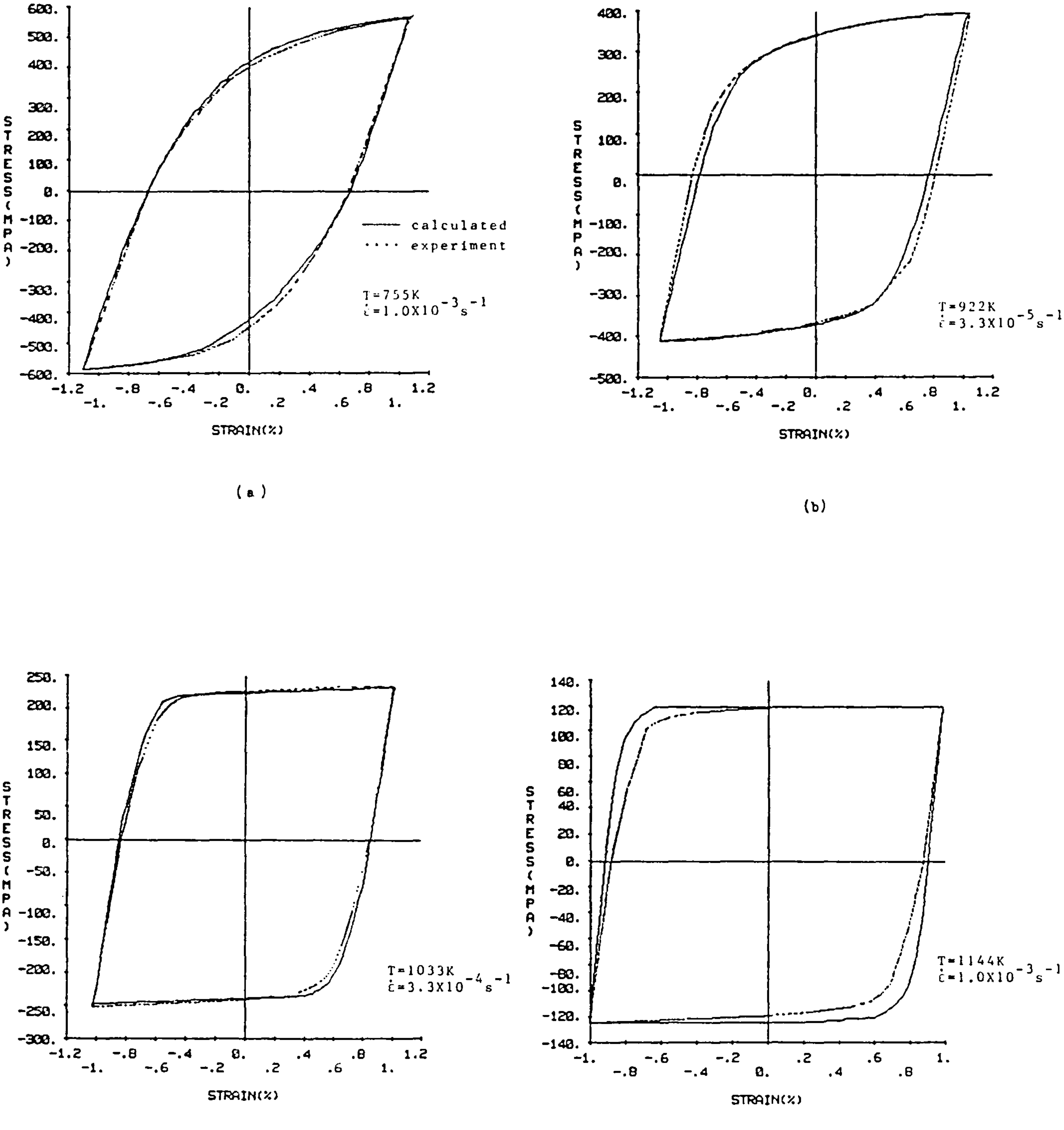

Figure 5. Stress/total strain hysteresis loops as measured and as calculated for Hastelloy-X at several different temperatures and strain rates.

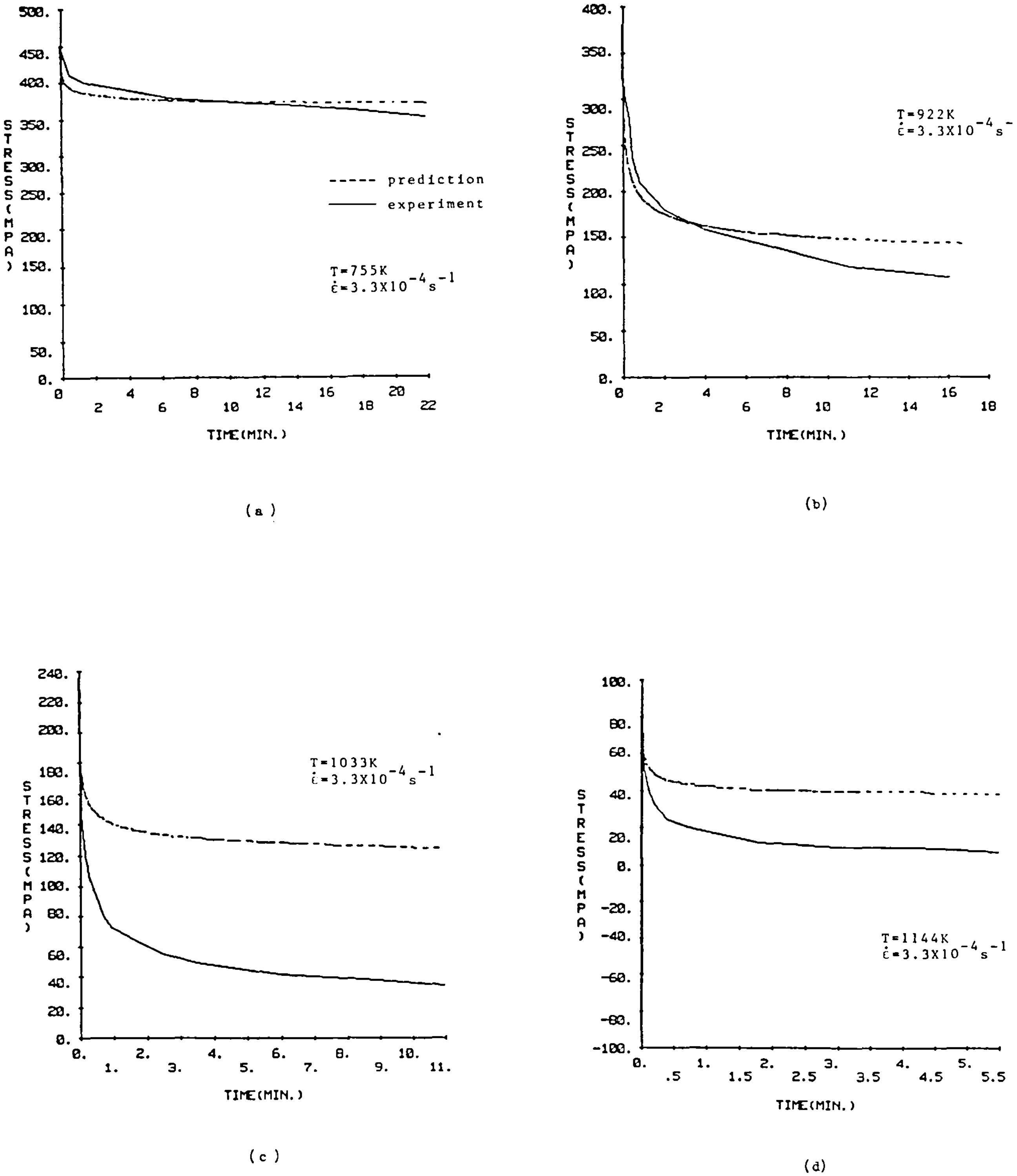

Figure 6. Stress relaxation behavior of Hastelloy-X as predicted by model and as measured experimentally.